chemistry

MDPI

Communication

Single-Ion Magnetism in a Three-Dimensional Thiocyanate-Bridged Dysprosium(III) Framework

Qingyun Wan [1,2,*,†], Mirosław Arczyński [1,3,†], Masanori Wakizaka [1,*], Shraddha Gupta [1], Nobuto Funakoshi [1] and Masahiro Yamashita [1,4,*]

[1] Department of Chemistry, Graduate School of Science, Tohoku University, Aramaki-Aza-Aoba, Aoba-Ku, Sendai 980-8578, Japan; miroslaw.arczynski@uj.edu.pl (M.A.); gupta.shraddha07@gmail.com (S.G.); nobuto.funakoshi.e7@tohoku.ac.jp (N.F.)
[2] State Key Laboratory of Synthetic Chemistry, HKU-CAS Joint Laboratory on New Materials, Department of Chemistry, The University of Hong Kong, Pokfulam Road, Hong Kong, China
[3] Faculty of Chemistry, Jagiellonian University, Gronostajowa 2, 30-387 Kraków, Poland
[4] School of Materials Science and Engineering, Nankai University, Tianjin 300350, China
* Correspondence: qywan@connect.hku.hk (Q.W.); masanori.wakizaka.a7@tohoku.ac.jp (M.W.); yamasita@agnus.chem.tohoku.ac.jp (M.Y.); Tel.: +81-22-765-6544 (M.Y.)
† These authors contributed equally to this work.

Abstract: New three-dimensional (3D) lanthanide framework compounds supported by bridging thiocyanate ligand and K^+ cations, $K_4[Ln(NCS)_4(H_2O)_4](NCS)_3(H_2O)_2$(**1:** Ln = Dy, **2:** Ln = Tb, **3:** Ln = Gd) have been synthesized. A single-crystal X-ray diffraction study showed that all three compounds were isostructural and crystallized in the I 2/a space group. The K^+ ion form 2D layers with thiocyanates which are further linked by $[Ln(NCS)_4(H_2O)_4]^-$ complexes and additional thiocyanate ions to generate an interesting 3D framework structure. Compound **1** shows slow magnetic relaxation behavior under a zero direct current (DC) field, indicating that **1** behaves as a single-ion magnet (SIM). As estimated from AC magnetic measurements, the effective energy barrier for spin reversal in 1 was U_{eff} = 42 cm^{-1}. Slow relaxation of magnetization under a small external DC field was also detected for 2 and 3 at 1.8 K.

Keywords: Dy(III); 3D coordination framework; SIM

Citation: Wan, Q.; Arczyński, M.; Wakizaka, M.; Gupta, S.; Funakoshi, N.; Yamashita, M. Single-Ion Magnetism in a Three-Dimensional Thiocyanate-Bridged Dysprosium(III) Framework. *Chemistry* **2023**, *5*, 987–995. https://doi.org/10.3390/chemistry5020067

Academic Editors: Zoi Lada and Konstantis Konidaris

Received: 18 March 2023
Revised: 24 April 2023
Accepted: 24 April 2023
Published: 26 April 2023

1. Introduction

Single-molecule magnets (SMMs) and single-ion magnets (SIMs) are usually composed of 3d and/or 4f discrete complexes with significant energy barriers to prevent spin reversal behaviors at the molecular levels [1–4]. SMMs/SIMs show promising applications such as high-density information storage, quantum computer, and molecular spintronics [1–3]. The large magnetic moments and remarkable magnetic anisotropy of lanthanide ions, particularly for the Dy^{3+} ions, make them potential candidates for SMMs/SIMs [3,5]. However, in the literature, most lanthanide SMMs/SIMs are based on isolated polynuclear or mononuclear complexes, and few Ln-type coordination frameworks are reported to behave as SMMs/SIMs so far [6–14].

Compared to discrete molecules, metal-coordination frameworks have higher structural stability, and this advantage has been utilized in constructing some metamagnetic materials [15,16]. However, slow magnetic relaxations in most of these framework compounds are absent due to the existence of 3D ordered exchange interactions among metal ions such as Ru and Co in the coordination framework [15–17]. For lanthanide coordination frameworks, the exchange interactions between lanthanide ions are usually weak, as the shielding of unpaired electrons in the 4f orbitals is strong [18]. We considered that such weak interatomic exchange interactions in Ln-frameworks can be utilized to promote the appearance of slow magnetic relaxation behaviors, leading to the efficient construction of SMMs/SIMs based on rigid and stable Ln-frameworks.

Some lanthanide metal-organic frameworks (MOFs) have been reported in the literature, where the organic linkers are usually made by carboxylate-type ligands [19]. Thiocyanate is a versatile inorganic ligand with a delocalized charge and polarizable π system [20,21]. Moreover, thiocyanate has two donor atoms of nitrogen and sulfur, which can coordinate with metals, leading to the formation of homo- or hetero-metallic MOF involving various combinations of metal ion node points, such as Cu-thiocyanate coordination polymer [20], Zn-K-thiocyanate MOF [22], Cd-thiocyanate MOF [23], Cd-Hg-thiocyanate and Mn-Hg-thiocyanate coordination polymers [21], and so on. These combinations lead to the formation of materials with interesting solid-state structures and hetero-metallic arrays. In the present work, we report three new Dy^{3+}, Tb^{3+}, and Gd^{3+} based coordination frameworks linked by inorganic SCN ligands and K^+ ions. To the best of our knowledge, this is the first report of Dy-type coordination framework bridged by thiocyanate ligands [24]. By examining its magnetic measurement, we found that **1** shows SIM properties with slow magnetic relaxation behavior under a zero DC field.

2. Materials and Methods

2.1. Synthesis

$LnCl_3 \cdot 6H_2O$ (Ln = Dy, Tb, Gd), potassium thiocyanate salts, and organic solvents were of analytical quality, commercially purchased, and used without any further purification.

$LnCl_3 \cdot 6H_2O$ (1 mmol) and potassium thiocyanate (7 mmol) were mixed with 10 mL of MeOH and stirred in an ultrasound bath for 10 min (Scheme 1). To precipitate KCl completely, the resulting white suspension was diluted with 110 mL of acetone and stirred for another 30 min. The resulting solution with white, slowly settling KCl precipitate was filtered. Filtrate was evaporated at a rotary evaporator to a slightly wet white precipitate. This product was dissolved in 1 mL of H_2O, transferred to a small petri dish, and recrystallized by evaporation of water. Due to high solubility in water, crystals form only when a very small amount of solvent remains. Therefore, the product is not filtered, but the obtained large transparent needle crystals are crushed and transferred as a wet slurry to a filter paper, where they are pressed against a paper to remove the remaining mother liquor. The collected product was dried in air to obtain **1**, **2,** or **3**. A yield of approximately 0.5 g, 60% (based on $LnCl_3 \cdot 6H_2O$) is obtained for all studied lanthanides. Elemental analysis: (**1**) $C_7H_{12}S_7N_7O_6DyK_4$, Calcd. (%): C, 10.09; H, 1.45; N, 11.76. Found (%): C, 10.109; H, 1.474; N, 11.819. (**2**) $C_7H_{12}S_7N_7O_6TbK_4$, Calcd. (%): C, 10.13; H, 1.46; N, 11.81. Found (%): C, 10.203; H, 1.555; N, 11.982. (**3**) $C_7H_{12}S_7N_7O_6GdK_4$, Calcd. (%): C, 10.15; H, 1.46; N, 11.84. Found (%): C, 10.242; H, 1.468; N, 11.898.

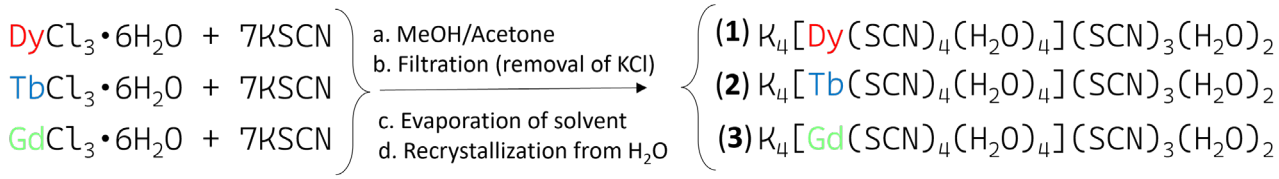

Scheme 1. Synthesis of the Ln-framework of **1**–**3**.

Compounds **1**, **2** and **3** subjected to a vacuum lose an unidentified number of water molecules. Samples partially rehydrated when exposed to air. Elemental analysis of dehydrated in vacuum and then rehydrated in air compounds: (**1**) (by missing one water molecule) $C_7H_{10}S_7N_7O_5DyK_4$, Calcd. (%): C, 10.31; H, 1.24; N, 12.02. Found (%): C, 10.388; H, 0.844; N, 12.210. (**2**) (by missing one water molecule) $C_7H_{10}S_7N_7O_5TbK_4$, Calcd. (%): C, 10.35; H, 1.24; N, 12.08. Found (%): C, 10.281; H, 1.188; N, 12.043. (**3**) (by missing two water molecules) $C_7H_8S_7N_7O_4GdK_4$, Calcd. (%): C, 10.61; H, 1.02; N, 12.38. Found (%): C, 10.675; H, 0.788; N, 12.445.

2.2. Physical Measurements

Single-crystal X-ray crystallographic data of compound **1**–**3** were collected at 120 K on equipment of a Rigaku Saturn 70 CCD Diffractometer (Rigaku, Tokyo, Japan) with graphite-monochromated Mo Kα radiation (λ = 0.71073 Å) produced by a VariMax microfocus X-ray rotating anode source. Data processing was performed using the Crystal-Clear crystallographic software package. The structures were solved using direct methods of SIR-92, and the refinement was carried out using SHELXL-2013 [25–27]. The non-H atoms were refined anisotropically using weighted full-matrix least squares, and H atoms attached to the O atoms were positioned using idealized geometries and refined using a riding model.

Powder X-ray diffraction measurements were performed on a Rigaku Smart Lab diffractometer equipped with a plate stage using Cu Kα radiation source (λ = 1.5456 Å) in a range 2θ = 3–60° before presentation data were corrected for background and Kα2 secondary reflections.

Magnetic measurements were performed using a magnetic property measurement system (MPMS-XL, Quantum Design, Baton Rouge, LA, USA) in the DC mode and the alternating current (AC) mode. Sample of compound 2 was measured in an RSO mode. The samples were measured in gelatin capsules (Matsuya). They were mixed with a small amount of melted eicosane (melting point = 37 °C) to additionally immobilize the samples and protect them from loss of crystalline solvent molecules during the measurement. The gelatin capsule was glued to a straw with a small piece of Kapton tape.

The elemental analysis was performed using J-Science Lab Co. Ltd. JM11 in collaboration with the Research and Analytical Center for Giant Molecules (Tohoku Univ.).

Fourier transform infrared spectra (FTIR) of powdered air-dried samples of 1, 2, and 3 were measured on a Jasco FT/IR-4200 equipped with an ATR PR0450-S system over a range of 4000–500 cm^{-1}. For ATR (attenuated total reflection), a diamond crystal was used with a 1.5 mm diameter of the sample contact area. KSCN spectra (Wako guaranteed reagent) were also measured for comparison with compounds **1**–**3**. The results were presented and discussed, in the context of SCN vibrations, in supporting information in Figures S10 and S11.

Continuous Shape Measure Analysis (CSHM) of all lanthanide ions in 1, 2 and 3 residing in eight-coordinate environments was performed using SHAPE program [28–30].

3. Results

3.1. Crystal Structures

Compounds **1**–**3** are isostructural and crystallize in the same I 2/a (15) space group (Tables S1–S3). The structures will be described using the **1** as an example. Bond lengths of Ln complexes in **1**, **2,** and **3** can be found in ESI Tables S7, S8, and S9, respectively. The crystal structure of compound **1** is shown in Figure 1. The framework is composed of the Dy cation, K cation, thiocyanate anion, and water molecules. The Dy atom is eight-coordinated, where the coordinated ligands include four NCS ligands and four water molecules (Figure 2).

The asymmetric unit (ASU) comprises only half of the Dy ion and its ligands (Figure S1). The other half can be obtained by rotation around the C_2 axis running through Dy ion along the crystallographic *b* axis. Apart from the Dy complex, ASU contains two potassium ions, K1 and K2, four thiocyanates, and three water molecules. Two water molecules are coordinated to Dy and one is in contact with K1 and K2 atoms. In following discussion, four thiocyanate ions, contained in the asymmetric unit will be referred to by the number 1, 2, 3, and 4, which reflects the atom label in the CIF file and presented figures (i.e., thiocyanate 4 is made of atoms labeled S4 N4 and C4). Thiocyanates 1 and 2 are coordinated by the N atom to Dy ions (Figure 2). As presented in Figure 1b, thiocyanate 3 bridges multiple K ions: two K1 and one K2 on the N side and furthermore one K1 and one K2 on the S side (note that in Figure 1b atoms K1 and K2 are shown with distinctive colors).

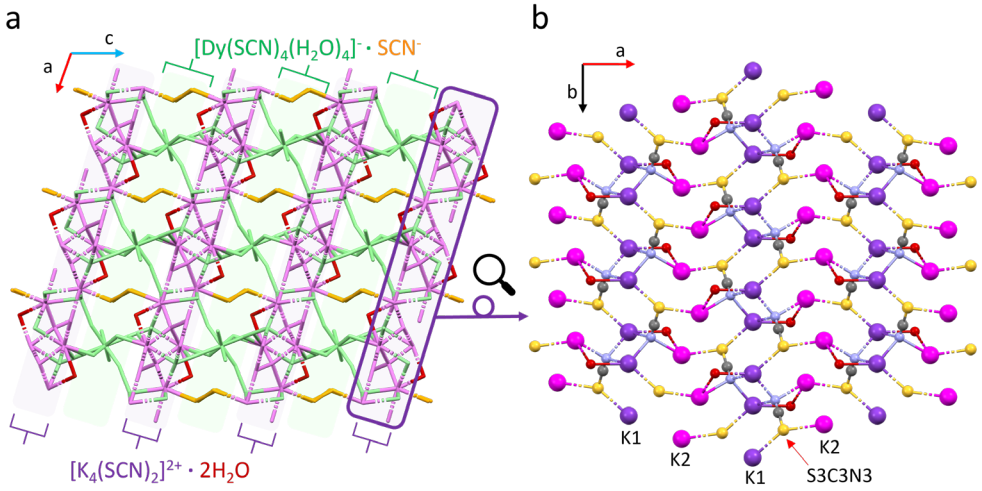

Figure 1. Structural motifs identified in 3D frameworks are reported here. (**a**). Crystal structure view along the *b*-axis. Particular components of the crystal structure are color coded for better clarity: $[Dy(SCN)_4(H_2O)_4]^-$ green; S4, C4, N4 orange; O3 red; K1, K2, S3, C3, N3 violet. Single $[K_4(SCN)_2]^{2+}$ layer viewed along the c-axis (**b**). Purple atom: K1, magenta K2, yellow: S3, grey: C3, blue: N3, red: O3. For clarity, $[Dy(SCN)_4(H_2O)_4]^-$ complexes, thiocyanate 4 (atoms S4, C4, N4) and H atoms were omitted.

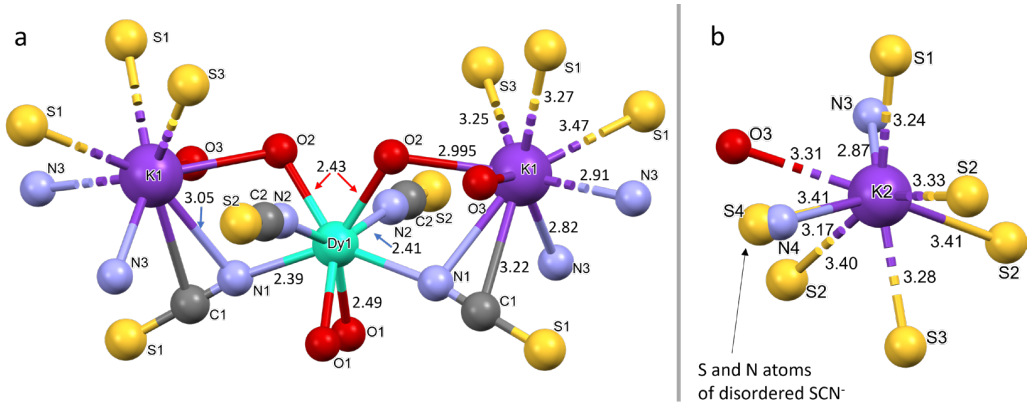

Figure 2. Geometry of the Dy complex and potassium K1 ions (**a**) geometry of K2 ions (**b**). The bond lengths are given in Å.

Potassium ions are assembled around thiocyanate 3, forming a distinctive $[K_4(SCN)_2]^{2+}$ layer (Figure 1a,b). This layer spreads across *a* and *b* crystallographic directions and is supported from the sides by other thiocyanates as well as water molecules present in the structure (Figure 1a). Thiocyanate number 4 is only partially 50% occupied and reveals a disorder in which the N and S ends of the molecule exchange positions with a 50% probability. This thiocyanate stretches between and bridges two neighboring $[K_4(SCN)_2]^{2+}$ layers by bonding to potassium K2 atoms. This arrangement is clearly illustrated in Figure 1a with the orange color of bridging thiocyanate 4, purple color of $[K_4(SCN)_2]^{2+}$ layers, and green $[Dy(SCN)_4(H_2O)_4]^-$ complexes. The red color in Figure 1 highlights uncoordinated water molecules on the Dy atom.

As shown in Figure 2a, for the Ln coordination geometry, the distance between Dy and coordinating N atoms is 2.39 and 2.41 Å, and the Dy-O distance is 2.49 and 2.43 Å. K1 cation interacts with the S and N atoms of the thiocyanate ligands, with the K1-S distance falling in the range of 3.25 to 3.47 Å and the shortest K-N distance of 2.82 Å (Figure 2a). The K1-O3 distance is 3.08 Å, while K2-O3 is 3.31 Å (Figure 2a,b). The shortest distances between Dy centers in the framework are 10.7 and 11.1 Å, along the a and c axis, respectively. The shortest distances between K1 centers is 4.82 Å and 4.03 Å along the a and c axis,

respectively. The shortest distance between K2 atoms is 4.82 Å, while it is 4.52 Å between K1 and K2.

3.2. Magnetic Properties

Direct current (DC) magnetic susceptibilities of polycrystalline samples **1**, **2**, and **3** were measured in the range of 1.8–300 K at the magnetic field of 0.1 T. As shown in Figure 3a, the χT values around room temperature are 15 cm^3 K mol^{-1} (**1**), 11 cm^3 K mol^{-1} (**2**), and 7.9 cm^3 K mol^{-1} (**3**), which is consistent with those of the single ions of Dy^{3+} ($^6H_{15/2}$: $J = 15/2$ and $g_J = 4/3$), Tb^{3+} ($^7F_6$: $J = 6$ and $g_J = 3/2$), and Gd^{3+} ($^8S_{7/2}$: $J = 7/2$ and $g_J = 2$), respectively [3]. The decrease of the χT of **1** and **2** when lowering the temperature is considered to be due to the thermal depopulation of the sublevel excited states of Ln^{3+} ions [6], which mainly relates to zero-field splitting. Additionally, antiferromagnetic interactions between Ln^{3+} ions are considered to be relatively weak due to the efficient shielding effect of unpaired electrons in the Ln-4f orbitals, thereby making small contributions to the magnetization process. Please note that the small increase of χT around 10 K in **3** and 17 K in **2** and **3** is a measurement artifact due to "emu-range" change, not a property of the samples [31]. The magnetization-field loops show no visible hysteresis at 1.8 K in all compounds (Figure 3b).

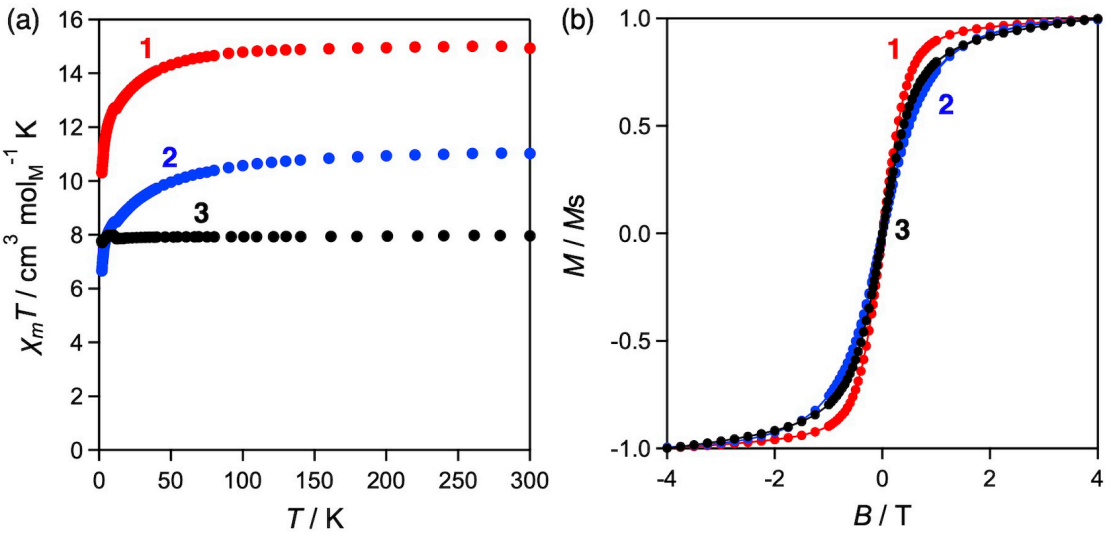

Figure 3. Plots of (**a**) χT vs. T and (**b**) normalized magnetization (M/M_S)-field loops at 1.8 K for **1** (red), **2** (blue), and **3** (black).

Alternating current magnetic susceptibilities of **1**, **2**, and **3** were measured for the study of their SIM behaviors. The Tb and Gd framework compounds **2** and **3** show slow magnetic relaxation but only under a magnetic field (Figure S1). At zero magnetic field, no slow magnetic relaxation phenomenon was observed for these two systems. Additionally, these two compounds show multiple Debye relaxations under a magnetic DC field, indicating the existence of second faster magnetic relaxation processes. Recently, in similar case, one of the two relaxation processes observed in the $[Gd(phendo)_4]^{3+}$ complex was shown to fade away upon dilution with diamagnetic Y^{3+} ions, suggesting that it was due to correlated spin movements arising from the dipole–dipole interactions between Gd^{3+} ions [32]. It was suggested that Gd^{3+} complexes might be good qubit candidates. Similar behavior of **3** is expected; however, we did not pursue that research pathway here. All in all, compounds **2** and **3** are not desirable SIM materials. On the other hand, for compound **1,** shown in Figure 4 and Figure S2, clear peaks appeared in the frequency dependence of the out-of-phase (χ″) susceptibilities in the range of 1.8–4.5 K at zero fields (Figure 4a) and in the range of 3.0–4.5 K at the magnetic field of 0.1 T (Figure 4b). The peaks in the frequency dependence χ″ plot indicate the SIM behaviors of compound **1**.

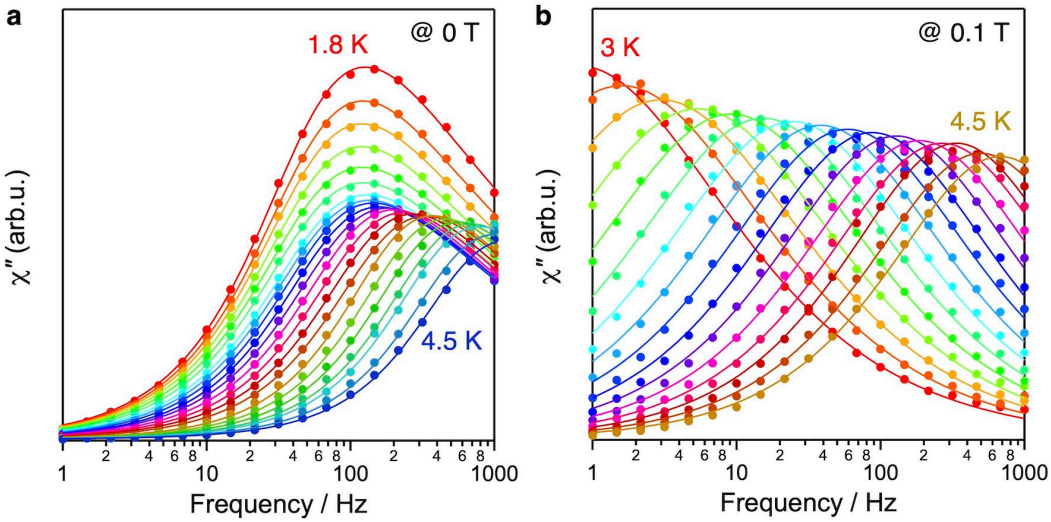

Figure 4. Frequency dependence of the out-of-phase magnetic susceptibility χ″ at (**a**) zero field in the temperature range of 1.8–4.5 K, and (**b**) 0.1 T in the temperature range of 3–4.5 K of compound **1**.

Curve fitting was carried out using the Debye relaxation model (Equation (1)) for 0.1 T and Havriliak–Negami model (Equations (2) and (3)) for zero-field [33]:

$$\chi''(\omega) = \frac{(\chi_T - \chi_S)(\omega\tau)^{1-\alpha}\cos(\pi\alpha/2)}{1 + 2(\omega\tau)^{1-\alpha}\sin(\pi\alpha/2) + (\omega\tau)^{2-2\alpha}} \quad (1)$$

$$\chi''(\omega) = \frac{(\chi_T - \chi_S)\sin(\beta\theta)}{[1 + 2(\omega\tau)^{1-\alpha}\sin(\pi\alpha/2) + (\omega\tau)^{2-2\alpha}]^{\beta/2}} \quad (2)$$

$$\theta = tan^{-1}\frac{(\omega\tau)^{1-\alpha}\cos(\pi\alpha/2)}{1 + (\omega\tau)^{1-\alpha}\sin(\pi\alpha/2)} \quad (3)$$

where ω (= $2\pi f$), f, χ_T, χ_S, τ, α and β refer to the AC angular frequency and the AC frequency, isothermal susceptibility, adiabatic susceptibility, relaxation time, dispersion coefficient, and asymmetric coefficient, respectively. These fitting parameters are summarized in Tables S4 and S5. The fitting at 0.1 T was carried out using a Debye relaxation model. On the other hand, the plots measured at zero-field show asymmetric peaks that require a Havriliak–Negami model with β. At the high-temperature region (>3.9 K), the parameter of β was assumed from the tendency of the plot at the near temperature region (~3.9 K, Figure S3) and fixed during the fitting (Table S4) because the opposite side of the peak was out of the measurement range. This assumption was appropriate, as the relaxation time plots converged at a higher temperature region with/without field (vide infra).

Figure 5 shows the Arrhenius plots of the relaxation times of compound **1**. The Arrhenius plot (blue line) measured under an applied field of 0.1 T shows a straight line, indicating that compound **1** follows the magnetic relaxation of the Orbach process (Equation (4)):

$$\tau_{Orbach} = \tau_0 \exp\left(\frac{U_{eff}}{k_B T}\right) \quad (4)$$

where τ_0, U_{eff}, and k_B refer to the preexponential activation energy of spin-reversal, and Boltzmann constant, respectively. The linear fitting affords U_{eff} = 42 cm^{-1} and $\tau_0 = 3.6 \times 10^{-10}$ s. The τ_0 of **1** is a typical value for the SMMs/SIMs with a relaxation time of 10^{-6} to 10^{-11} s [34]. At zero-field, the red plot curve shows nearly constant relaxation time at a temperature below around 3 K, suggesting the existence of quantum tunneling magnetization (QTM) at low temperatures [35,36].

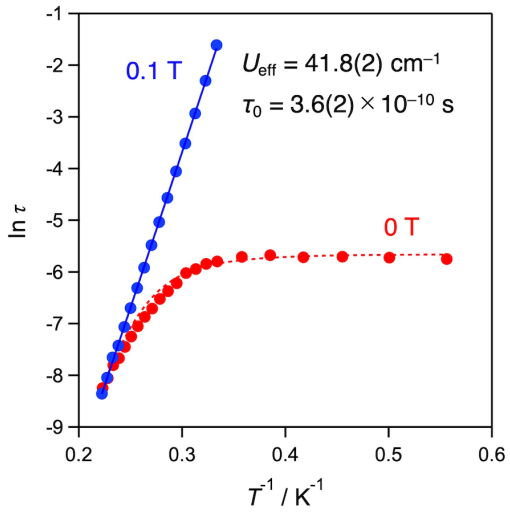

Figure 5. Plots of ln(τ) versus 1/T for **1** at 0.1 and 0 T, the solid blue line and the red dotted line represent the best fit with the Arrhenius law and the simulation with U_{eff} = 41.8 cm^{-1}, τ_0 = 3.6 × 10^{-10} s, C = 40 K^7 s, and Q = 0.0035 s, respectively.

The red plot of Figure 5 measured under zero-field can be simulated using a combination of the Orbach, Raman, and QTM processes (Equations (5)–(7)):

$$\tau_{Raman} = CT^{-7} \quad (5)$$

$$\tau_{QTM} = Q \quad (6)$$

$$\tau^{-1} = {\tau_{Orbach}}^{-1} + {\tau_{Raman}}^{-1} + {\tau_{QTM}}^{-1} \quad (7)$$

where *C* and *Q* refer to the coefficient of the Raman and QTM processes, respectively, the red line at the low-temperature region is distinctly different from the straight line measured at 0.1 T, indicating that applying the magnetic field effectively suppresses the Raman and QTM processes of **1**. These results clearly indicate that Dy(III) ions in **1** perform as SIMs with thermo-activation energy. It should be noted that the studied compounds could be partially dehydrated due to the vacuum conditions of the magnetic measurements. The effect of hydration/de-hydration on the magnetism of compounds **1**, **2,** and **3** was not studied at this stage. Further research in this direction is required and will be conducted in the future.

4. Conclusions

In summary, we have successfully synthesized three Dy/Tb/Gd frameworks linked by thiocyanate ligands. Magnetic investigations reveal that the Dy(III) ion in a framework compound **1** behaves as SIM, showing suppression of the Raman and the quantum tunneling magnetization processes by applying a magnetic field.

Supplementary Materials: The following supporting information can be downloaded at: https://www.mdpi.com/article/10.3390/chemistry5020067/s1. Table S1. Crystal data and structure refinement for **1** at 120 K. CCDC: 2249738. Table S2. Crystal data and structure refinement for **2** at 120 K. CCDC: 2249739. Table S3. Crystal data and structure refinement for **3** at 120 K. CCDC: 2249740. Figure S1. Asymmetric unit of 1. Figure S2. The real part (χ') and the imaginary part (χ'') of AC susceptibility of (a, b) **2** and (c, d) **3**, measured at 1.8 K under the magnetic field of 0, 0.1, and 0.2 T. The curve lines for χ'' show a dual Debye model. Figure S3. The real part of AC magnetic susceptibility (χ') of **1** under the static magnetic field of 0 T and 0.1 T, respectively. Table S4. AC susceptibility fitting data of the imaginary part of **1** at 0 T. Table S5. AC susceptibility fitting data of the imaginary part of **1** at 0.1 T. Figure S4. Plots of the temperature dependence of b of **1** at 0 T fitted using Equations (2) and (3) in the manuscript. Figure S5. Crystal structure of compound **1**–**3**

along (a) a-, (b) b- and (c) c-axis. Figure S6. PXRD pattern of compounds **1, 2,** and **3** measured at 293 K—crystals were ground before measurements. Figure S7. Comparison of calculated (on the basis of single crystal structural data at 120 K) and measured (at 293 K) PXRD patterns of compound **1**. Figure S8. Comparison of calculated (on the basis of single crystal structural data at 120 K) and measured (at 293 K) PXRD patterns of compound **2**. Figure S9. Comparison of calculated (on the basis of single crystal structural data at 120 K) and measured (at 293 K) PXRD patterns of compound **3**. Table S6. Bond lengths of Dy1, K1, and K2 centers. Table S7. Bond lengths of Tb1, K1, and K2 centers. Table S8. Bond lengths of Gd1, K1, and K2 centers. Table S9. Results of the continuous shape measure analysis of lanthanide ion coordination spheres in compounds **1**, **2**, and **3** and symmetry of the corresponding ideal shapes. Figure S10. IR spectra of 1 (red), 2 (blue), 3 (green), and KSCN (black) in the range of 4000–500 cm^{-1}. Selected vibration peaks are marked. Figure S11. IR spectra of 1 (red), 2 (blue), 3 (green), and KSCN (black) in the range of 2200–1900 cm^{-1}. Selected vibration peaks are marked. References [28–30,37] are cited in the supplementary materials.

Author Contributions: M.Y. conceived and designed the experiments; M.W., Q.W., S.G., M.A. and N.F. performed the experiments; M.W., Q.W., S.G., M.A. and N.F. analyzed the data; Q.W. and M.W. wrote the paper. All authors have read and agreed to the published version of the manuscript.

Funding: This work was supported by the JSPS KAKENHI Grant Number JP19H05631 and the National Natural Science Foundation of China (NSFC, 22150710513). M.Y. thanks the 111 projects (B18030) from China.

Data Availability Statement: Data is contained within the article and Supplementary Materials.

Acknowledgments: W.Q. thanks the support from Chi-Ming Che at the University of Hong Kong.

Conflicts of Interest: The authors declare no conflict of interest.

References

1. Sessoli, R.; Gatteschi, D.; Caneschi, A.; Novak, M. Magnetic bistability in a metal-ion cluster. *Nature* **1993**, *365*, 141–143. [CrossRef]
2. Gatteschi, D.; Sessoli, R. Quantum tunneling of magnetization and related phenomena in molecular materials. *Angew. Chem. Int. Ed.* **2003**, *42*, 268–297. [CrossRef]
3. Woodruff, D.N.; Winpenny, R.E.; Layfield, R.A. Lanthanide single-molecule magnets. *Chem. Rev.* **2013**, *113*, 5110–5148. [CrossRef] [PubMed]
4. Yamashita, M. Next generation multifunctional nano-science of advanced metal complexes with quantum effect and nonlinearity. *Bull. Chem. Soc. Jpn.* **2021**, *94*, 209–264. [CrossRef]
5. Zhang, P.; Guo, Y.-N.; Tang, J. Recent advances in dysprosium-based single molecule magnets: Structural overview and synthetic strategies. *Coord. Chem. Rev.* **2013**, *257*, 1728–1763. [CrossRef]
6. Liu, C.-M.; Zhang, D.-Q.; Zhu, D.-B. A 3D MOF constructed from dysprosium (III) oxalate and capping ligands: Ferromagnetic coupling and field-induced two-step magnetic relaxation. *Chem. Commun.* **2016**, *52*, 4804–4807. [CrossRef]
7. Chen, M.; Sañudo, E.C.; Jimenez, E.; Fang, S.-M.; Liu, C.-S.; Du, M. Lanthanide–organic coordination frameworks showing new 5-connected network topology and 3D ordered array of single-molecular magnet behavior in the Dy case. *Inorg. Chem.* **2014**, *53*, 6708–6714. [CrossRef] [PubMed]
8. Yi, X.; Calvez, G.; Daiguebonne, C.; Guillou, O.; Bernot, K. Rational organization of lanthanide-based SMM dimers into three-dimensional networks. *Inorg. Chem.* **2015**, *54*, 5213–5219. [CrossRef]
9. Huang, H.; Gao, W.; Zhang, X.-M.; Zhou, A.-M.; Liu, J.-P. 3D Ln III-MOFs: Displaying slow magnetic relaxation and highly sensitive luminescence sensing of alkylamines. *CrystEngComm* **2019**, *21*, 694–702. [CrossRef]
10. Hu, F.-L.; Jiang, F.-L.; Zheng, J.; Wu, M.-Y.; Pang, J.-D.; Hong, M.-C. Magnetic properties of 3D heptanuclear lanthanide frameworks supported by mixed ligands. *Inorg. Chem.* **2015**, *54*, 6081–6083. [CrossRef]
11. Savard, D.; Lin, P.-H.; Burchell, T.J.; Korobkov, I.; Wernsdorfer, W.; Clérac, R.; Murugesu, M. Two-dimensional networks of lanthanide cubane-shaped dumbbells. *Inorg. Chem.* **2009**, *48*, 11748–11754. [CrossRef]
12. Yin, D.-D.; Chen, Q.; Meng, Y.-S.; Sun, H.-L.; Zhang, Y.-Q.; Gao, S. Slow magnetic relaxation in a novel carboxylate/oxalate/hydroxyl bridged dysprosium layer. *Chem. Sci.* **2015**, *6*, 3095–3101. [CrossRef] [PubMed]
13. Zhou, Q.; Yang, F.; Xin, B.; Zeng, G.; Zhou, X.; Liu, K.; Ma, D.; Li, G.; Shi, Z.; Feng, S. Reversible switching of slow magnetic relaxation in a classic lanthanide metal–organic framework system. *Chem. Commun.* **2013**, *49*, 8244–8246. [CrossRef] [PubMed]
14. Zhang, X.; Vieru, V.; Feng, X.; Liu, J.L.; Zhang, Z.; Na, B.; Shi, W.; Wang, B.W.; Powell, A.K.; Chibotaru, L.F. Influence of Guest Exchange on the Magnetization Dynamics of Dilanthanide Single-Molecule-Magnet Nodes within a Metal-Organic Framework. *Angew. Chem. Int. Ed.* **2015**, *54*, 9861–9865. [CrossRef]
15. Motokawa, N.; Matsunaga, S.; Takaishi, S.; Miyasaka, H.; Yamashita, M.; Dunbar, K.R. Reversible magnetism between an antiferromagnet and a ferromagnet related to solvation/desolvation in a robust layered $[Ru_2]_2TCNQ$ charge-transfer system. *J. Am. Chem. Soc.* **2010**, *132*, 11943–11951. [CrossRef]

16. Cheng, X.-N.; Zhang, W.-X.; Chen, X.-M. Single crystal-to-single crystal transformation from ferromagnetic discrete molecules to a spin-canting antiferromagnetic layer. *J. Am. Chem. Soc.* **2007**, *129*, 15738–15739. [CrossRef]
17. Espallargas, G.M.; Coronado, E. Magnetic functionalities in MOFs: From the framework to the pore. *Chem. Soc. Rev.* **2018**, *47*, 533–557. [CrossRef]
18. Ishikawa, N.; Sugita, M.; Wernsdorfer, W. Nuclear spin driven quantum tunneling of magnetization in a new lanthanide single-molecule magnet: Bis (phthalocyaninato) holmium anion. *J. Am. Chem. Soc.* **2005**, *127*, 3650–3651. [CrossRef] [PubMed]
19. Cui, Y.; Chen, B.; Qian, G. Lanthanide metal-organic frameworks for luminescent sensing and light-emitting applications. *Coord. Chem. Rev.* **2014**, *273*, 76–86. [CrossRef]
20. Nagarkar, S.S.; Kurasho, H.; Duong, N.T.; Nishiyama, Y.; Kitagawa, S.; Horike, S. Crystal melting and glass formation in copper thiocyanate based coordination polymers. *Chem. Commun.* **2019**, *55*, 5455–5458. [CrossRef]
21. Jin, F.; Zhou, H.-P.; Wang, X.-C.; Hu, Z.-J.; Wu, J.-Y.; Tian, Y.-P.; Jiang, M.-H. Synthesis, structures and photoluminescence of thiocyanate bridged metal-organic polymers containing functional imidazole ligand. *Polyhedron* **2007**, *26*, 1338–1346. [CrossRef]
22. Abedi, M.; Mahmoudi, G.; Kirillov, A.M.; Kaminsky, W. Self-Assembled 3D heterometallic Zn (II)/K (I) metal–organic framework with the fluorite topology. *Polyhedron* **2018**, *142*, 110–114. [CrossRef]
23. Etaiw, S.E.-d.H.; El-bendary, M.M.; Fouda, A.E.-A.S.; Maher, M.M. A new metal-organic framework based on cadmium thiocyanate and 6-methylequinoline as corrosion inhibitor for copper in 1 M HCl solution. *Prot. Met. Phys. Chem. Surf.* **2017**, *53*, 937–949. [CrossRef]
24. Lozano-Rodriguez, M.; Copping, R.; Petit, S.; Solari, P.; Guilbaud, P.; de Leon, J.M.; Den Auwer, C. Crystal structure versus solution for two new lutetium thiocyanato complexes. *N. J. Chem.* **2011**, *35*, 2755–2765. [CrossRef]
25. Altomare, A.; Burla, M.C.; Camalli, M.; Cascarano, G.L.; Giacovazzo, C.; Guagliardi, A.; Moliterni, A.G.; Polidori, G.; Spagna, R. SIR97: A new tool for crystal structure determination and refinement. *J. Appl. Crystallogr.* **1999**, *32*, 115–119. [CrossRef]
26. Farrugia, L.J. WinGX and ORTEP for Windows: An update. *J. Appl. Crystallogr.* **2012**, *45*, 849–854. [CrossRef]
27. Sheldrick, G.M. Crystal structure refinement with SHELXL. *Acta Crystallogr. Sect. C Struct. Chem.* **2015**, *71*, 3–8. [CrossRef] [PubMed]
28. Pinsky, M.; Avnir, D. Continuous symmetry measures. 5. The classical polyhedra. *Inorg. Chem.* **1998**, *37*, 5575–5582. [CrossRef]
29. Casanova, D.; Cirera, J.; Llunell, M.; Alemany, P.; Avnir, D.; Alvarez, S. Minimal distortion pathways in polyhe-dral rearrangements. *J. Am. Chem. Soc.* **2004**, *126*, 1755–1763. [CrossRef]
30. Cirera, J.; Ruiz, E.; Alvarez, S. Shape and Spin State in Four-Coordinate Transition-Metal Complexes: The Case of the d6 Configuration. *Chem.—Eur. J.* **2006**, *12*, 3162–3167. [CrossRef] [PubMed]
31. Ney, A.; Kammermeier, T.; Ney, V.; Ollefs, K.; Ye, S. Limitations of measuring small magnetic signals of samples deposited on a diamagnetic substrate. *J. Magn. Magn. Mater.* **2008**, *320*, 3341–3346. [CrossRef]
32. Handzlik, G.; Magott, M.; Arczyński, M.; Sheveleva, A.M.; Tuna, F.; Sarewicz, M.; Osyczka, A.; Rams, M.; Vieru, V.; Chibotaru, L.F. Magnetization dynamics and coherent spin manipulation of a propeller Gd (III) complex with the smallest helicene ligand. *J. Phys. Chem. Lett.* **2020**, *11*, 1508–1515. [CrossRef] [PubMed]
33. Topping, C.; Blundell, S. AC susceptibility as a probe of low-frequency magnetic dynamics. *J. Phys. Condens. Matter* **2018**, *31*, 013001. [CrossRef] [PubMed]
34. Liu, C.-M.; Xiong, J.; Zhang, D.-Q.; Wang, B.-W.; Zhu, D.-B. Multiple thermal magnetic relaxation in a two-dimensional ferromagnetic dysprosium (III) metal–organic framework. *RSC Adv.* **2015**, *5*, 104854–104861. [CrossRef]
35. Borah, A.; Murugavel, R. Magnetic relaxation in single-ion magnets formed by less-studied lanthanide ions Ce (III), Nd (III), Gd (III), Ho (III), Tm (II/III) and Yb (III). *Coord. Chem. Rev.* **2022**, *453*, 214288. [CrossRef]
36. Feltham, H.L.; Brooker, S. Review of purely 4f and mixed-metal nd-4f single-molecule magnets containing only one lanthanide ion. *Coord. Chem. Rev.* **2014**, *276*, 1–33. [CrossRef]
37. Seki, T.; Chiang, K.-Y.; Yu, C.-C.; Yu, X.; Okuno, M.; Hunger, J.; Nagata, Y.; Bonn, M. The bending mode of water: A powerful probe for hydrogen bond structure of aqueous systems. *J. Phys. Chem. Lett.* **2020**, *11*, 8459–8469. [CrossRef]